EPTT 2024
Escola de Primavera de Transição e Turbulência

ABCM
Associação Brasileira de Engenharia e Ciências Mecânicas

EPTT-2024-0007
STABILITY OF LIQUID SHEETS IN FUEL INJECTORS

Igor S. Paccini
Marcio T. Mendonca
Fernando S. Costa
Instituto Nacional de Pesquisas Espaciais
igorspaccini@gmail.com, marcio_tm@yahoo.com, fernando.costa@inpe.br

Abstract. *Liquid propellants are one of the main sources of energy used in rocket engines. Propellant injectors are responsible for the atomization of fuel and oxidizer in order to increase their vaporization rates and promote proper mixing and burning in a short distance to reduce combustor length and weight. The atomization takes place through the growth of disturbances that breakup the liquid sheet coming out of the injector. The present article describes a study of stability analysis of liquid sheets and the corresponding estimate for the sheet breakup length. The analysis is based on the solution of the analytical dispersion relation for conic sheets for a range of Weber numbers, which relates inertia and surface tension effects. Breakup length is determined for the fastest growing wavenumber and frequency where an empirical correlation is used to correlate total amplification and breakup length. Results show a good correlation between theoretical breakup length and experimental results when the azimuthal velocity used in the dispersion relation is lower than the velocity estimated from correlations for the given injectors used in the experiments.*

Keywords: *fuel injectors, hydrodynamic stability, liquid sheets, breakup length, atomization, spray formation*

1. INTRODUCTION

Pressure swirl injectors are commonly used in gas turbine combustor, industrial burners, rocket engines and various other engineering fields. These devices convert enthalpy into kinetic energy to achieve a high relative velocity of the liquid compared to the surrounding gas, using channels or ports tangentially positioned to promote a swirl in the fluid, a chamber and a nozzle. The liquid spreads out after exiting the injector nozzle forming a conical sheet due to the centrifugal force. Fig. 1 presents a typical hollow cone spray, which is a feature of pressure swirl atomizers.

The liquid enters a swirl chamber through tangential ports that give it a high angular velocity, creating an air-cored vortex (Dash *et al.*, 2001; Kang *et al.*, 2018) . This swirling motion pushes the liquid against the chamber walls, causing it to exit the nozzle as a thin sheet near the nozzle exit, which then spreads radially outward to form a hollow cone spray. The fuel is injected at high speed, and the liquid sheet becomes susceptible to the Kelvin-Helmholtz instability due to the significant velocity difference between the liquid sheet and the surrounding air (Han *et al.*, 1997; Marchione *et al.*, 2007). Trying to explain the early stages of the instabilities, Dombrowski and Hooper (1962) studied the influence of the aerodynamic forces on the instabilities and disintegration of viscous liquid sheets, giving more details of how it starts and relating largest growth rate to the corresponding wave number. This instability leads to the breakup of the liquid sheet into ligaments, as shown in the Fig. 1, and subsequently into droplets, forming a well-defined hollow cone spray. The atomization process in swirl injectors is driven not only by the breakup of the liquid sheet but also by droplet collisions and interactions between the drops and the air.

The theory of hydrodynamic stability examines how a laminar flow responds to disturbances of small or moderate amplitude. A flow is considered stable if it returns to its original laminar state after being disturbed, and unstable if the disturbance grows and alters the laminar flow into a different state Kundu and Cohen (2008). While instabilities can lead to turbulent motion, they might also transform the flow into another, typically more complex, laminar state (Schmid and Henningson, 2001). Stability theory involves the mathematical analysis of disturbances superimposed on a laminar base flow. Often, these disturbances are assumed to be small, allowing for further simplifications, such as using linear equations to describe their evolution. When disturbance velocities exceed a few percent of the base flow, nonlinear effects become significant, and linear equations lose their predictive accuracy. Despite their limitations, linear equations are crucial for identifying physical growth mechanisms and dominant disturbance types. This approach is effective for predicting the behavior of instabilities and parameters like breakup length, spray cone angle, droplet sizes, and spray velocities Almeida Machado *et al.* (2023). Some applications of linear stability theory include controlling laminar flow on the wings of aircraft to reduce fuel consumption, predicting transition locations from laminar to turbulent and optimizing jet

flows for more efficient combustion in gas turbines and internal combustion engines.

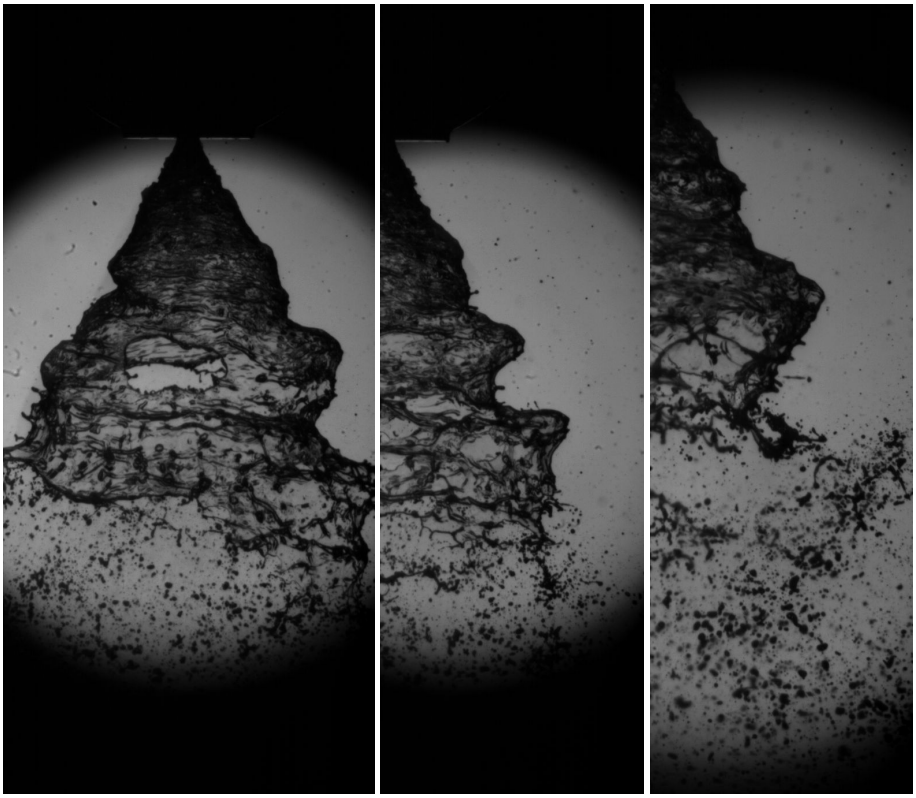

Figure 1. Spray cone ejected from the pressure swirl atomizer.

Kinematic effects are crucial in open flows and can independently cause instabilities. Inviscid flows that have an inflection point in the base velocity profile are unstable acording to Rayleigh's criterion Kundu *et al.* (2015). On the other hand, base flow velocity profiles without inflection points can only become unstable through delicate feedback mechanisms involving viscous momentum transfer and vorticity diffusion.

Understanding the break up mechanisms is crucial for the continuous development of injector designs that meet the demand for better efficiency and contributes to the current need to reduce polluting gases. The study of instabilities in spray atomization is also essential for optimizing a wide range of industrial processes, improving environmental impact and promoting innovation in various sectors. It has direct implications for efficiency, product quality and safety in countless applications. Understanding instabilities helps in designing atomizers that produce sprays with consistent and desirable characteristics.

This paper centers on a theoretical approach to examine how the maximum growth rate and corresponding wavenumber affect the breakup length. Concurrently, experimental results were obtained to validate our initial conclusions and ensure that the experimental methods can reliably reproduce them. Additionally, the study underscores the significance of using optical diagnostic techniques to visualize emerging instabilities and the breakup process. This study uses optical diagnostic techniques and a high-speed video camera to measure droplet velocities, breakup length, spray cone angle, and droplet size. The spray cone angle generated by pressure swirl atomizers is particularly important for combustion systems, as it significantly affects ignition performance, flame blowout limits, and emissions of unburned hydrocarbons. Consequently, potential unsteady behaviors from such nozzles are crucial, as they can trigger other oscillations that may destabilize the entire combustion process. Fluctuations in fuel flow rate cause variations in the heat release rate, leading to combustion instabilities in many systems Harrje (1972).

2. METHODOLOGY

The main concern of the hydrodynamic stability is to investigate the breakdown of laminar flows, their development and eventual transition to turbulent flow regime. Evolution of small oscillations traveling in laminar boundary-layers was first discussed by Rayleigh, Lefebvre and McDonell (2017). Linear stability theory deals with the first stage of the transition process, starting from the appearance of small sinusoidal disturbances in the otherwise undisturbed laminar flow until nonlinear interactions between amplified disturbances start occurring. In this paper, the Linear Stability Theory is outlined resulting in the stability equations and the final dispersion equation. The theory was applied for a three-

dimensional, steady, inviscid, incompressible mean flow. Initially a conical flow configuration was considered, however the formulation became too complex and consequently a cylindrical coflow configuration was assumed. Many studies contributed to the description of the initial propagation of the instabilities considering plannar (Dombrowski and Hooper, 1962) and (Ashgriz and Yarin, 2011), cylindrical (Abu-Nabah, 2003) and (Ibrahim and Jog, 2006) and even conical liquid sheets Fu *et al.* (2010). The formulation of the conical liquid sheet in (Fu *et al.*, 2010), are not clear.

Next the linear stability analysis will be discussed considering small disturbances on an annular liquid sheet under three dimensional disturbances. Normal modes solutions will be sought for the linearized disturbances equations.

2.1 Formulation of the Linear Stability Theory

In order to perform the stability analysis it is assumed that the liquid sheet is annular with a coflow of inner and outer gas streams. The geometrical and flow conditions are shown in Fig. 2. The liquid and gas phases are assumed to be inviscid and incompressible as mentioned before. A parallel flow will be assumed. The velocities for the inner gas, outer gas and liquid sheet are given respectively by $(U_i, 0, 0), (U_o, 0, 0)$ and $(U_l, 0, W_r)$. Where U is the axial velocity for the liquid sheet and for the surrounding gas. They have different directions. V is the radial velocity and is zero and W_r is the tangential velocity. R_a and R_b are the inner and outer radius of the liquid sheet. η_i and η_0 are the displacements amplitudes of the liquid sheet. Notice that the axial velocity is in the same direction of the x coordinate, while the inner and outer axial velocities of the surrounding air are opposite to it. The same can be seen for the tangential velocities $W_{l,i,o}$.

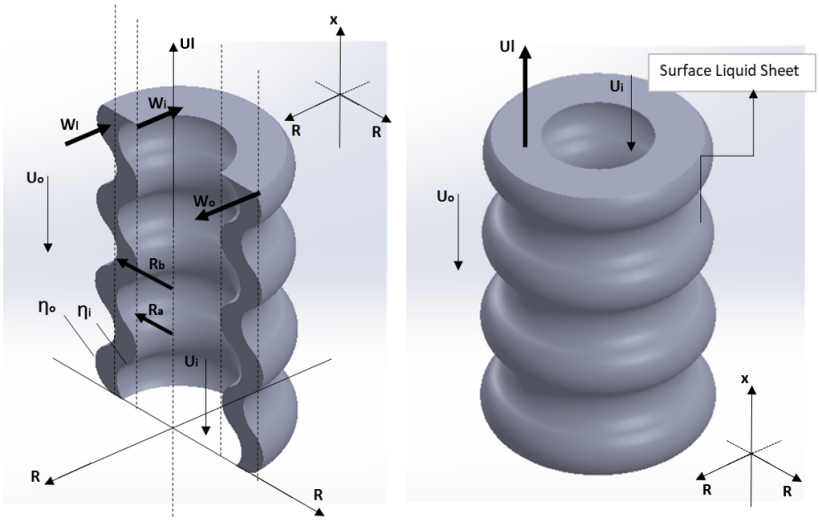

Figure 2. Representation of an annular liquid sheet and its components.

The governing equations in a cylindrical coordinate system are the continuity equation:

$$\frac{\partial U}{\partial x} + \frac{V}{r} + \frac{\partial V}{\partial r} + \frac{1}{r}\frac{\partial W}{\partial \theta} = 0, \tag{1}$$

and the momentum equations,

$$\begin{aligned}
&\frac{\partial U}{\partial t} + U\frac{\partial U}{\partial x} + V\frac{\partial U}{\partial r} + \frac{W}{r}\frac{\partial U}{\partial \theta} + = -\frac{1}{\rho}\frac{dp}{dx}, \\
&\frac{\partial V}{\partial t} + U\frac{\partial V}{\partial x} + V\frac{\partial V}{\partial r} + \frac{W}{r}\frac{\partial V}{\partial \theta} - \frac{W^2}{r} = -\frac{1}{\rho}\frac{dp}{dr}, \\
&\frac{\partial W}{\partial t} + U\frac{\partial W}{\partial x} + V\frac{\partial W}{\partial r} + \frac{W}{r}\frac{\partial W}{\partial \theta} + \frac{VW}{r} = -\frac{1}{\rho r}\frac{dp}{d\theta}.
\end{aligned} \tag{2}$$

The method of small disturbances simplifies the analysis of complex nonlinear problems by introducing small disturbances to a known base flow or equilibrium state, leading to a linear problem because it makes use of linearization techniques. The velocity components are decomposed as:

$$U = \overline{U} + u, \qquad V = v, \qquad W = \overline{W} + w, \qquad p = P + p'. \tag{3}$$

The arguments with over bar and upper case represent the assumed base flow quantities and the prime and lower case indicates disturbance. A normal mode solution assumes that each component of the perturbation can be expressed as a product of a complex amplitude and an oscillatory function. The general form for a normal mode solution is:

$$(u, v, w, p') = (\hat{u}(r), \hat{v}(r), \hat{w}(r), \hat{p}(r)) \exp i(kx + n\theta - \omega t) + cc, \tag{4}$$

where, the disturbances were written in the complex plane and cc stands for the complex conjugate.

- (u, v, w, p') are the perturbations to the base flow.
- $(\hat{u}, \hat{v}, \hat{w}, \hat{p'})$ are the amplitude functions that only depend on the radial coordinate r. These complex functions represent disturbances amplitude and phase.
- k is the stream wise wavenumber and n is the spanwise wavenumber.
- ω is the complex frequency, which includes both the oscillation frequency (real part) and the growth/decay rate (imaginary part).

For the temporal instability analysis, the wave number k and n are real while frequency ω is complex. The imaginary part of ω reflects the growth rate of the disturbance. If ω has a positive imaginary part, the disturbances grow exponentially, indicating instability. If the imaginary part is negative, the disturbances decay, indicating stability. The choice of a complex frequency ω and real wave numbers is known as the temporal problem where the spatial structure of the wavelike disturbances are unchanged and the amplitude of the wave grows or decays as time progresses.

The primary condition to apply normal modes solutions is that the system must be linear and homogeneous, at least with respect to the disturbances. Normal modes solutions decompose disturbances into sinusoidal components, simplifying the analysis of linearized equations. The method is applicable under conditions of linearity, homogeneity, and appropriate boundary conditions. It's an important technique in linear stability analysis, providing insights into the stability of various physical systems. The displacement disturbances at the inner and outer interfaces are given by:

$$\eta_0(x, \theta, t) = \eta_0 \exp i(kx + n\theta - \omega t) \tag{5}$$

$$\eta_i(x, \theta, t) = \eta_i \exp i(kx + n\theta - \omega t) \tag{6}$$

Substituting eq. 4 into the eq. 1 and the eq. 2 and neglecting second order terms, we get the linearized disturbance equations for the liquid flow.

Continuity equation:

$$\frac{\partial u}{\partial x} + \frac{v}{r} + \frac{\partial v}{\partial r} + \frac{1}{r}\frac{\partial w}{\partial \theta} + = 0. \tag{7}$$

Momentum equations:

$$\frac{\partial u}{\partial t} + U_l \frac{\partial u}{\partial x} + \frac{W_j}{r}\frac{\partial u}{\partial \theta} = -\frac{1}{\rho_j}\frac{\partial p'_j}{\partial x}, \tag{8}$$

$$\frac{\partial v}{\partial t} + U_l \frac{\partial v}{\partial x} + \frac{W_j}{r}\frac{\partial v}{\partial \theta} - 2\frac{W_j w}{r} = -\frac{1}{\rho_j}\frac{\partial p'_j}{\partial r}, \tag{9}$$

$$\frac{\partial w}{\partial t} + U_l \frac{\partial w}{\partial x} + v\frac{\partial W_j}{\partial r} + \frac{W_j}{r}\frac{\partial w}{\partial \theta} + 2\frac{W_j v}{r} = -\frac{1}{\rho_j r}\frac{\partial p'_j}{\partial \theta}. \tag{10}$$

where $j = i, o$ and $W_i = \Omega r, W_o = A_o/r$.

Boundary conditions need to be enforced at the liquid interface. The primary boundary condition is the kinematic condition, which states that a fluid particle on the surface must move with the surface. In other words, the velocity components perpendicular to the interface must be continuous across the interface.

For the gas streams:

$$v_i = \frac{D\eta_i}{Dt} = \frac{\partial \eta_i}{\partial t} + U_i \frac{\partial \eta_i}{\partial x} + \Omega \frac{\partial \eta_i}{\partial \theta} \qquad \text{at} \qquad r = R_a, \tag{11}$$

$$v_o = \frac{D\eta_o}{Dt} = \frac{\partial \eta_o}{\partial t} + U_o \frac{\partial \eta_o}{\partial x} + \frac{A_o}{r^2}\frac{\partial \eta_o}{\partial \theta} \qquad \text{at} \qquad r = R_b, \tag{12}$$

For the liquid phase:

$$v = \frac{D\eta_i}{Dt} = \frac{\partial \eta_i}{\partial t} + U_l \frac{\partial \eta_i}{\partial x} + \frac{A_l}{r^2}\frac{\partial \eta_i}{\partial \theta} \qquad \text{at} \qquad r = R_a, \tag{13}$$

$$v = \frac{D\eta_o}{Dt} = \frac{\partial \eta_o}{\partial t} + U_l \frac{\partial \eta_o}{\partial x} + \frac{A_l}{r^2}\frac{\partial \eta_i}{\partial \theta} \qquad at \qquad r = R_o. \tag{14}$$

The dynamic boundary condition relates the balance between the surface stresses on both sides of the liquid-gas interface, including the pressure jump across the interface due to surface tension. The effect of the viscous forces will be neglected, in order to simplify the problem. Then the expressions for the dynamic boundary conditions are:

$$p_l' - p_i' = \sigma(\frac{\eta_i}{R_a^2} + \frac{1}{R_a^2}\frac{\partial^2 \eta_i}{\partial \theta^2} + \frac{\partial^2 \eta_i}{\partial x^2}) - \frac{\rho_l A_l^2 \eta_i}{R_a^3} + \rho_i \Omega^2 R_a \eta_i, \tag{15}$$

$$p_l' - p_o' = -\sigma(\frac{\eta_o}{R_b^2} + \frac{1}{R_b^2}\frac{\partial^2 \eta_o}{\partial \theta^2} + \frac{\partial^2 \eta_o}{\partial x^2}) - \frac{\rho_l A_l^2 \eta_o}{R_b^3} + \frac{\rho_o A_o^2 \eta_o}{R_b^3}. \tag{16}$$

The two equations, eq.15 and eq.16 express the balance of the normal component of the stress tensor at each interface. After solving the linearized equations for liquid and gas we can obtain the liquid pressure, inner gas pressure and outer gas pressure. These development are presented in Abu-Nabah (2003) and Ibrahim (2006). Substituting these in the dynamic boundary conditions eq.15 and eq. 16, the problem then reduces to a system of two equations. By a series of mathematical simplification we end up with the final dispersion equation. The dispersion equation is non-dimensionalized by introducing the following dimensionless parameters:

$$\begin{gathered}
We_i = \frac{\rho_i U_i^2 R_b}{\sigma}, \qquad We_o = \frac{\rho_o U_o^2 R_b}{\sigma}, \qquad We_l = \frac{\rho_l U_l^2 R_b}{\sigma}, \\
We_{si} = \frac{\rho_i \Omega^2 R_b^3}{\sigma}, \qquad We_{so} = \frac{\rho_o A_o^2}{\sigma R_b}, \qquad We_{sl} = \frac{\rho_l A_l^2}{\sigma R_b}, \\
g_i = \frac{\rho_i}{\rho_l}, \qquad g_o = \frac{\rho_o}{\rho_l}, \qquad h_= \frac{R_a}{R_b}, \qquad \overline{k} = kR_b, \qquad \overline{\omega} = \frac{\omega R_b}{U_l}, \qquad \overline{k}_1 = \overline{k}\sqrt{1 - \frac{c_5}{(c_4 - \overline{\omega})^2}}.
\end{gathered} \tag{17}$$

The Weber number We relates inertia and surface tension in the different flow regions. Indexes (i, o, l) refer to the inner interface, outer interface and liquid sheet, ρ is the fluid density and σ the surface tension coefficient. The constants $R_a, R_b, A_l, A_o, h, g_i$ and g_0, are the characteristic parameters of the fluid, where Ra and Rb are the inner and outer radius of the liquid sheet. A_l, A_o are the inner and outer vortex strength, h is the ratio of the inner and outer radius and g_i and g_o are the inner and outer density ratios. The final dispersion equation is an fourth order equation of the form below:

$$c_7\overline{\omega}^4 + c_8\overline{\omega}^3 + c_9\overline{\omega}^2 + c_{10}\overline{\omega} + c_{11} - \frac{g_i\left(-c_1\overline{\omega}^4 + +c_{12}\overline{\omega}^3 + +c_{13}\overline{\omega}^2 + +c_{14}\overline{\omega} + c_{15}\right)}{c_{16}I_n(k\overline{k}_1) + (c_4 - \overline{\omega})\sqrt{1 - \frac{c_5}{(c_4-\overline{\omega})^2}}I_n'(h\overline{k_1})}(c_4 - \overline{\omega})\, I_n(h\overline{k}_1) = 0, \tag{18}$$

where the constants c_i with i going from 1 to 16 are given in Abu-Nabah (2003), and In represents the n-th order modified Bessel function of the first kind. The constants c_i are an agglomeration of other constants, allowing Eq. 18 to be written in a simpler form. In order to save space the expressions for c_i are not included in this paper. The modified Bessel functions are function of the wavenumber k and the radius r of the injector exit orifice.

The analysis consists in solving the dispersion relation numerically in order to find the relation between the wave number k, frequency ω_r and growth rate ω_i as a function of the non-dimensional parameters in order to find the fastest growing mode. The breakup length L is determined assuming an empirical correlation for the amplification $\log(\eta/\eta_0)$ and computing the breakup time τ (Fu, 2010),

$$\tau = \frac{\log(\eta/\eta_0)}{\omega_i}, \qquad L = V\tau = V\frac{\log(\eta/\eta_0)}{\omega_i}, \tag{19}$$

where an assumed value for $\log(\eta/\eta_0)$ is based on empirical data. Different authors suggest different values for $\log(\eta/\eta_0)$ ranging from 2 to 12, which depends on the type of injector and operating conditions. The term V is the axial velocity of the liquid sheet and τ is the break up time.

3. EXPERIMENTAL METHODOLOGY

In this section will be discussed briefly the experimental methodology, and how the data were acquired to be compared with the theoretical results. The experimental test bench is shown in Fig. 3.The test bench is composed by an air compressor, a reservoir or tank with 5 litres capacity, valves, pressure transducer, pressure swirl injectors, and water as a fluid simulating the liquid propellant. Besides that, optical diagnostics systems are used in the experimental setup to visualize the liquid sheet of the spray in high resolution. Water was pressurized from 0.1 to 0.6 MPa. The response frequency of the pressure transducer is 0 to 100 kHz, with the pressure transducer signal converted from 0-10 V to 4-20 mA. A high-speed Fastec digital camera was used to visualize the spray. Telecentric and microscopic shadowgraphy systems included lenses from Edmunds Optics company. The open source software ImageJ was used to analyse the collected frames. The acquisition system could record the spray at different frames per second, depending on the arrangement used. The data acquisition system can analyse the cone spray angle, droplets formation and measure the speed of the droplets. The measurements were taken by the ImageJ software which has a versatile configuration that enables measure- ment of the spray angle, velocities, droplets diameter and breakup length. The velocity was obtained accordingly with the frames per second of each recording. Knowing the frames per second, the same as frequency, it is possible to find the time between frames and then determine the velocity by multiplying the time for the distance the droplet has moved.

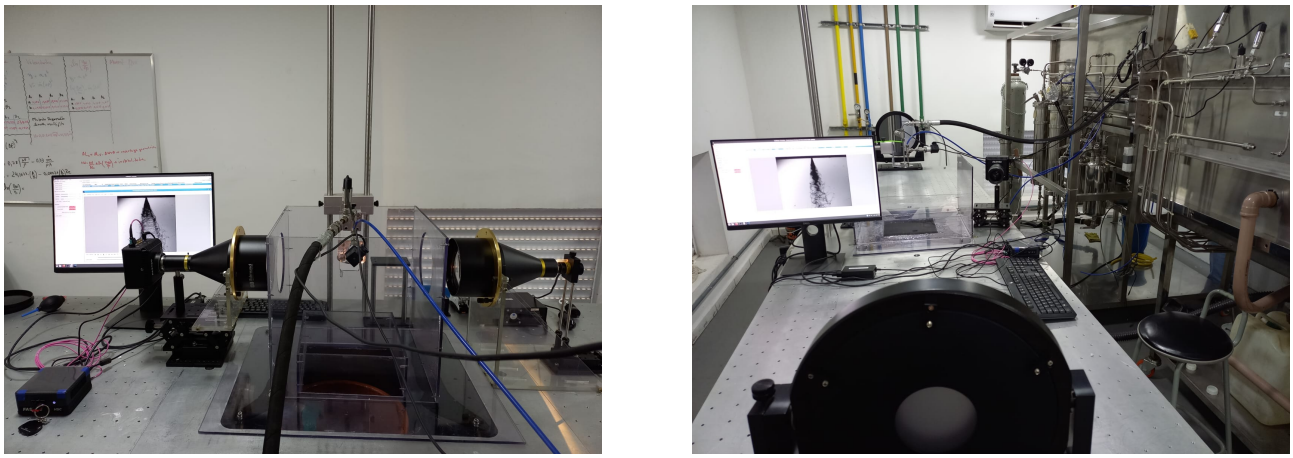

Figure 3. Test bench and the optical system installed.

The pressure swirl injector shown in Fig. 6 is made of stainless steel. A single model of this injector was considered, with three different exit orifices of 1mm, 1.5mm and 1.8mm. The features of this injector are also shown in Fig. 6. This pressure swirl atomizer is composed of two parts. The inner part has a thread in its body but not in all its radius and the outer part has its inner surface threaded and envelops the inner body. A gap is formed between the inner and outer component. The fluid flows through this channel and is forced to go inside to the next chamber, close to the exit. At the tip of the central body, it has 3 channels that will provide the swirl motion to the fluid, and when the fluid reaches there, it will rotate until emerges outside of the swirl chamber.

4. RESULTS AND DISCUSSIONS

To solve the dispersion equation, a numerical solution procedure was developed using the secant method. The algorithm identifies the four roots of the dispersion equation and selects the root with the largest imaginary part, corresponding to the disturbance largest growth rate, from which the associated wavenumber is determined. The real part corresponds to the angular frequency. An iterative loop varies the values of the non-dimensional wave number in small increments. The curves shown Fig. 5 display the solution of the dispersion equation, relating the non-dimensional growth rate and the non-dimensional wave number, for a fixed axial Weber number $W_{el} = 1079$ and considering four different values of the swirl Weber number, $W_{es} = 0, 2, 8$, and 20. Furthermore, the axial velocities of the gas were considered zero, for both of inner and outer gas ($U_{i,o} = 0$). This is because we haven't considered a flow of gas with a certain velocity contrary to the liquid sheet, but a stationary surrounding gas and the liquid sheet flowing through the gas.

According to Ibrahim and Jog (2006), the correlation between growth rate and breakup length should match the experimental breakup length, with different values for the axial and swirl Weber numbers providing an equally good match between the model and experimental results.

Initially, theoretical estimates of the velocity components of the spray suggested that the swirl velocity was of the same order as the axial velocity. However, the estimated swirl velocities did not match the experimental breakup lengths for the computed growth rates. Analysis of experimental images revealed that initial voids on the liquid sheets, corresponding to

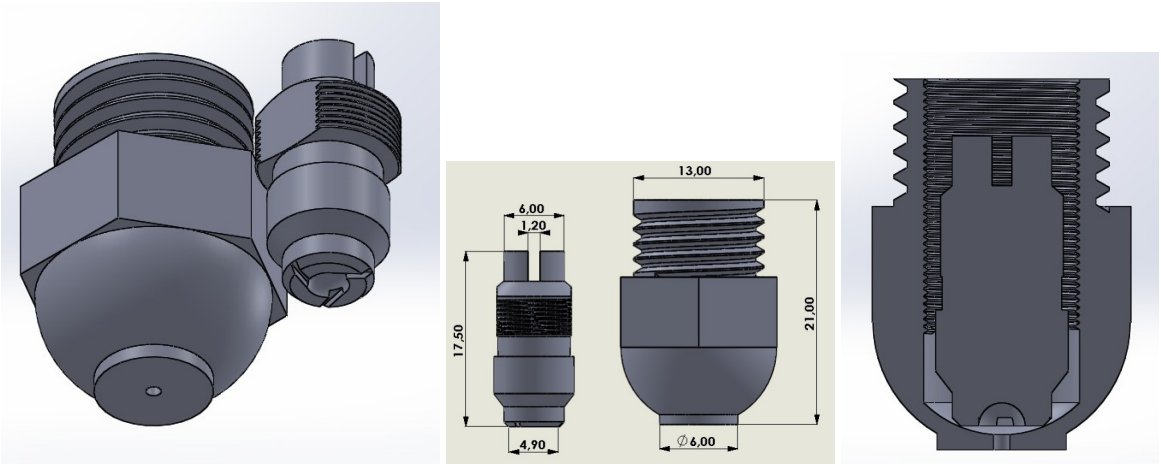

Figure 4. Injector geometry, dimensions and how it is assembled. The dimensions are all in millimeters.

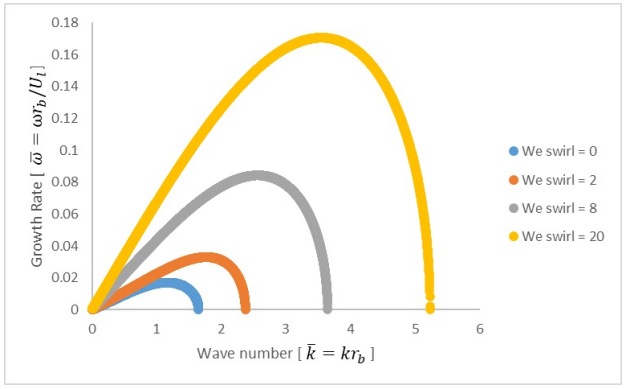

Figure 5. Growth rates variation with wavenumber for different values of Weber number.

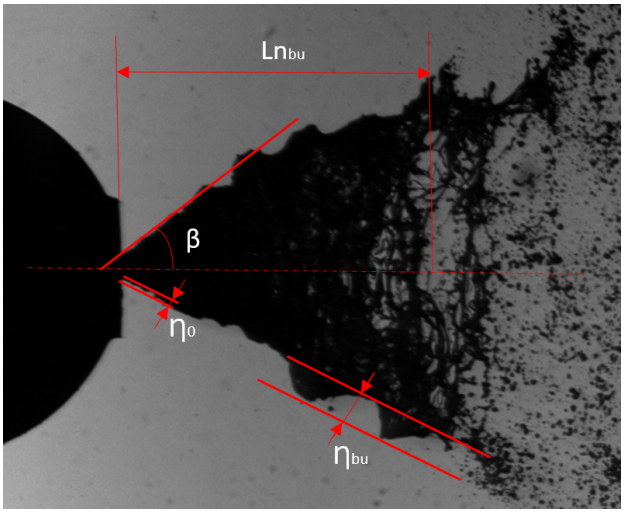

Figure 6. Image of a fuel injector spray showing the liquid film breakup.

initial breakup patches or holes, moved downstream with minimal rotation in the azimuthal direction, indicating that the swirl velocity was much lower than estimated.

Figure 7 shows a sequence of images capturing the formation of the first voids on the liquid sheet surface. The near zero swirl velocity was inferred from the almost straight path of these voids until complete breakup. The relationship between frames per second and resolution is inversely proportional, and the frame rate was adjusted to record four images capturing the beginning and total breakup of the liquid sheet.

Considering the experimental observation that the swirl velocities are very small, the resulting swirl Weber number is also small. Assuming swirl Weber numbers in the range of 0 to 20, the corresponding tangential velocities, according to Eq. 17, vary from 0 to 1.5 m/s. Table 1 summarizes the data collected from experiments for different injection pressures, showing theoretical and experimental axial velocities, the corresponding disturbance amplification $\ln(\eta/\eta_0)$, and the theoretical and experimental breakup lengths L_b. The growth rates were recalculated considering a low swirl velocity, resulting in a better match between the modeled breakup length and the experimental results, as shown in Fig. 8.

Figure 9 presents comparisons between theoretical and experimental axial velocities and breakup lengths at various inlet pressure levels. The agreement between theoretical and experimental values improves as the pressure increases. This improvement can be attributed to the fact that the theoretical model for axial velocity is more accurate at higher pressures.

Other inferences were made regarding the empirical breakup lengths calculated by Inamura *et al.* (2003),Inamura *et al.* (2001) and Fu *et al.* (2010). Kang *et al.* (2018), in their paper, they summarize a list of empirical formulations for breakup length, similar to what Lefebvre and McDonell (2017) does, presenting several expressions for this parameter. The equations from Inamura *et al.* (2003),Inamura *et al.* (2001) and Fu *et al.* (2010) used to evaluate the correlation with the data obtained experimentally and through the theoretical development with the solution of the dispersion equation are

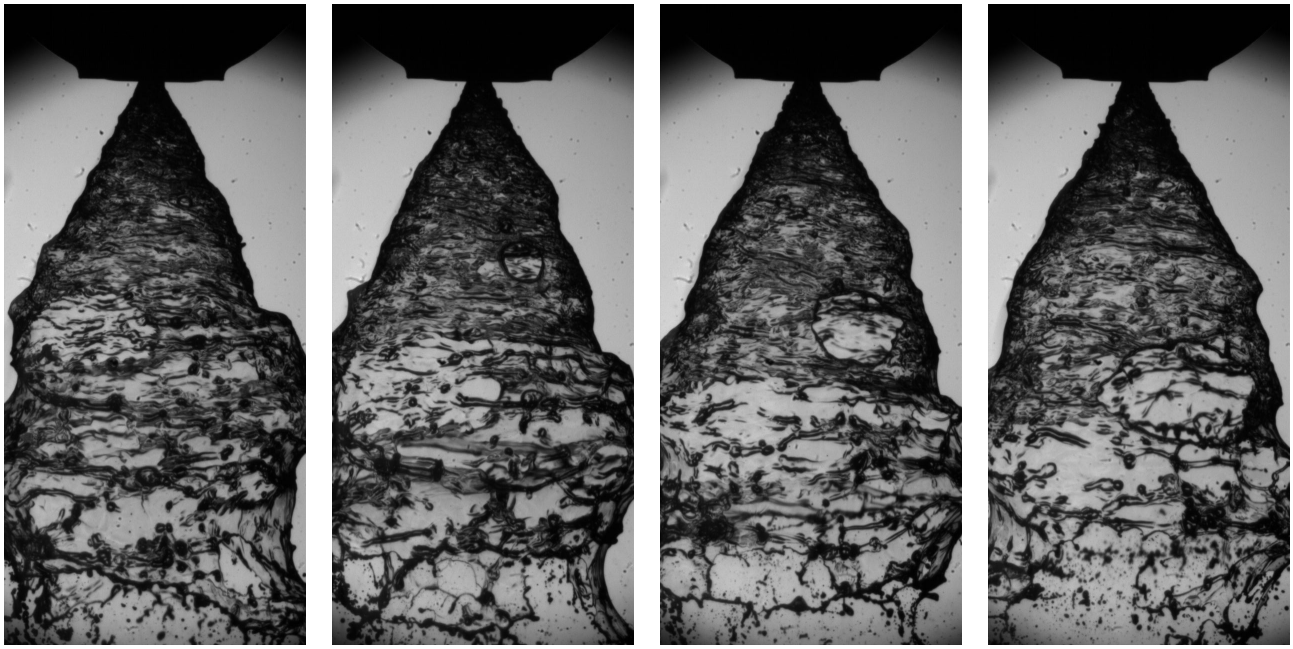

Figure 7. Voids beginning on the surface liquid sheet and following a straight path until breakup.

Table 1. Breakup lengths, axial velocities and disturbance amplifications for different injection pressures.

Pressure[MPa]	Axial Velocity$_1$[m/s]	Axial Velocity$_2$[m/s]	$\ln(\eta/\eta_0)$	$L_{b\ 1}$[mm]	$L_{b\ 2}$[mm]
0.1	1.26	12.56	2.42	1.74	17.42
0,15	8.93	14.06	2.52	10.02	15.17
0.20	12.56	16.10	2.76	10.76	14.35
0.25	15.36	17.99	2.48	10.59	14.09
0.30	17.71	17.91	2.88	14.24	12.68
0.35	19.78	20.50	2.47	11.89	11.83
0.40	21.65	20.98	2.65	13.66	12.31
0.45	23.37	22.25	2.57	9.64	10.63
0.50	24.97	22.59	2.56	9.45	10.68
0.55	26.47	24.59	2.55	9.14	10.29
0.60	27.89	26.19	2.56	9.07	9.18

$^{(1)}$ Theoretical, $^{(2)}$ Experimental

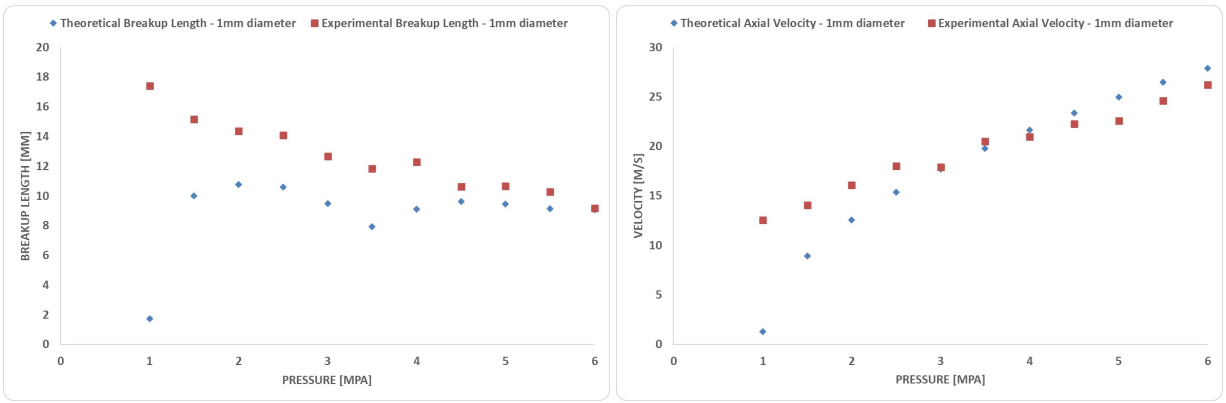

Figure 8. Comparison between theoretical and experimental axial velocity and corresponding breakup length for inlet pressures varying from 1 to 6 MPa.

shown bellow:

$$L_{bu} = 0.82[\frac{\rho_l \sigma \ln \frac{\eta_{bu}}{\eta_0} h_0 cos(\beta)}{\rho_g{}^2 U^2}]^{0.5} \tag{20}$$

$$L_{bu} = 0.2175[\frac{\rho_l \sigma \ln \frac{\eta_{bu}}{\eta_0} h_0 cos(\beta)}{\rho_g{}^2 U^2}]^{0.3} \tag{21}$$

where ρ_l and ρ_g are the density of the liquid and the surrounding gas, η_{bu} is the maximum amplitude at the breakup, η_0 is the initial amplitude, h_0 is the initial thickness of the liquid sheet at the orifice exit, β is the spray cone angle and U is the axial velocity. The calculation of each of these expressions takes into account the thickness of the liquid film at the injector's exit orifice. Both authors consider that the liquid film thickness decreases over time, that is, as the instability on the liquid surface increases, the thickness diminishes until it reaches its minimum value at the moment of breakup. For calculating the liquid film thickness at the injector orifice, a semi-empirical expression by Halder *et al.* (2001) was used to determine the air core diameter. After computing all the attributes associated with each expression, the results can be seen in Fig. 9, which relate the diameters of the three types of injectors used with the breakup lengths and pressure. The following equation is the Halder *et al.* (2001) empirical correlation to determine the air core diameter:

$$\frac{D_a}{D_0} = 0.338(1 - e^{-1.45x10^{-4}Re})\alpha^{0.073}(\frac{D_0}{D_s})^{0.424}(\frac{D_t}{D_s})^{-0.732}(\frac{L_0}{D_s})^{-0.252} \tag{22}$$

where D_a is the air core diameter, D_0 is the injector diameter, Re is the Reybolds number, α is the converge angle of the swirl chamber, D_s swirl chamber diameter, D_t tangential ports diameter and L_0 is the orifice lenght.

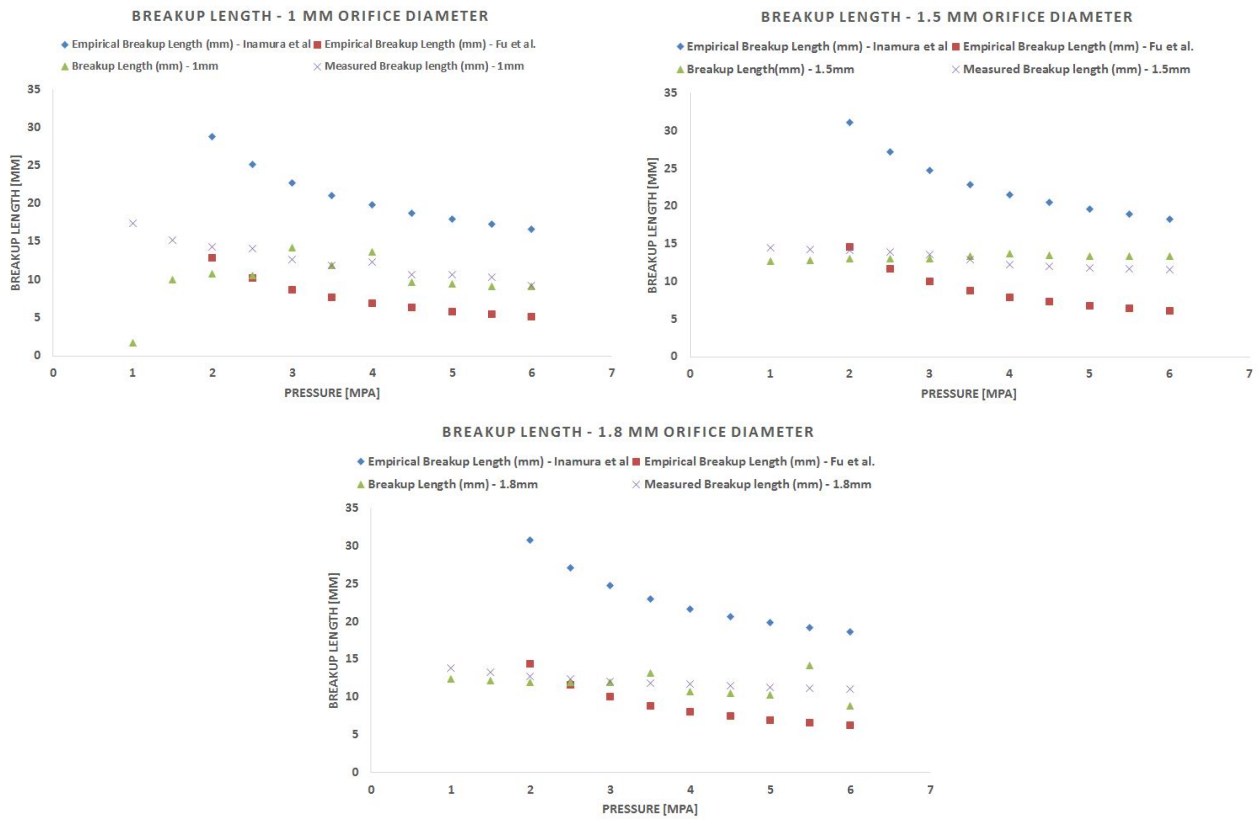

Figure 9. Comparison between three different orifice diameters, theoretical and experimental breakup length for inlet pressures varying from 1 to 6 MPa.

According to the graphs of Fig. 9, both expressions, Inamura *et al.* (2003),Inamura *et al.* (2001) and Fu *et al.* (2010), show little variation for different orifice diameters. The same pattern is observed for the measured breakup length values and the results obtained through modeling. Our results were overestimated compared to Fu *et al.* (2010) and underestimated compared to Inamura *et al.* (2003),Inamura *et al.* (2001). The images indicate a tendency for the breakup length to stabilize as the pressure increases. Another author that came through with similar results were Almeida Machado *et al.* (2023). In his paper, he uses a dual pressure swirl injector with different orifice diameters. His results about the breakup length show a tendency to stabilize as the pressure drop increases as well. Another interesting fact is the proximity of the ratio $\ln \frac{\eta_{bu}}{\eta_0}$. Almeida Machado *et al.* (2023), found values in the range of 2 to 3 for the ratio, the same interval as Fu *et al.* (2010), and this paper also found similar values. From the Table 1 is possible to follow this values for different droplet pressures, considering in this case 1mm diameter of the orifice.

5. CONCLUSIONS

A linear stability analysis of conical liquid sheets was conducted based on the derived dispersion relation. The determination of growth rates allow the estimate of breakup length for different flow conditions. Based on experimental observations, considering a lower spanwise Weber number, better agreement between experimental and estimated breakup lengths are obtained.

Comparison of theoretical and experimental results is important for the development and validation of old and new simulation models. In order to verify breakup length predictive modeling capability base on linear stability analysis pressure swirl injectors were tested under different operating conditions. The preliminary comparisons between theoretical and experimental results have shown significant discrepancies, since the pressure swirl injector model utilized yielded a very small swirl velocity. Therefore, by imposing low values for the swirl velocity in the stability and breakup length theoretical models, better comparisons with experimental results were obtained. The experimental observation about the magnitude of the swirl velocity was very important in order to obtain good comparisons between theoretical and experimental results. In conclusion, the correct identification of the flow parameters is required in order to feed the theoretical model, resulting in correct growth rates and values for the breakup length. The results also show that the injection pressure has a strong influence on the axial velocity and, therefore on the disturbances growth rate and breakup length. The tele- centric shadowgraphy system was crucial to understand and validate the magnitude of the velocity components (axial and azimuthal) on the conical jet coming out of the injector. For future works it would be interesting to analyse the influence of the radial velocity in the linear instability analysis model.

6. ACKNOWLEDGEMENTS

The authors acknowledge the financial support from CNPq, CAPES and FAPESP.

7. REFERENCES

Abu-Nabah, B., 2003. *Swirl Orientation Effect on the Instability and the Breakup of Annular Liquid Sheets*. Masterś thesis, University of Cincinnati.

Almeida Machado, D., Costa, F.S., Dias, G.S. and Mota, F.A., 2023. "Simultaneous analysis of liquid film instabilities and properties of swirl sprays by telecentric shadowgraphy". *Available at SSRN 4402991*.

Ashgriz, N. and Yarin, A., 2011. "Capillary instability of free liquid jets". *Handbook of Atomization and Sprays: Theory and Applications*, pp. 3–53.

Dash, S., Halder, M., Peric, M. and Som, S., 2001. "Formation of air core in nozzles with tangential entry". *J. Fluids Eng.*, Vol. 123, No. 4, pp. 829–835.

Dombrowski, N. and Hooper, P., 1962. "The effect of ambient density on drop formation in sprays". *Chemical Engineering Science*, Vol. 17, pp. 291–305.

Fu, Q.f., Yang, L.j., Qu, Y.y. and Gu, B., 2010. "Linear stability analysis of a conical liquid sheet". *Journal of Propulsion and Power*, Vol. 26, No. 5, pp. 955–968.

Halder, M., Dash, S. and Som, S., 2001. "Initiation of air core in a simplex nozzle and the effects of operating and geometrical parameters on its shape and size". *Therm. Fluid*.

Han, Z., Parrish, S.E., Farrell, P.V. and Reitz, R.D., 1997. "Modeling atomization processes of pressure-swirl hollow-cone fuel sprays". *Atomization and sprays*, Vol. 7, No. 6.

Harrje, D.T., 1972. *Liquid propellant rocket combustion instability*, Vol. 194. Scientific and Technical Information Office, National Aeronautics and Space ....

Ibrahim, A. and Jog, M., 2006. "Effect of liquid and air swirl strength and relative rotational direction on the instability of an annular liquid sheet". *Acta mechanica*, Vol. 186, pp. 113–133.

Ibrahim, A., 2006. *Comprehensive Study of Internal Flow Field and Linear and Nonlinear Instability of an Annular Liquid Sheet Emanating from an Atomizer*. Master's thesis, University of Cincinnati.

Inamura, T., Kei, M., Hiroshi, T. and Hiroshi, S., 2001. "Spray characteristics of swirl coaxial injector and its modeling". *37th Joint Propulsion Conference and Exhibit*.

Inamura, T., Tamura, H. and Sakamoto, H., 2003. "Characteristics of liquid film and spray injected from swirl coaxial injector." *Journal of Propulsion and Power*, Vol. 19, p. 632–639.

Kang, Z., Wang, Z.g., Li, Q. and Cheng, P., 2018. "Review on pressure swirl injector in liquid rocket engine". *Acta Astronautica*, Vol. 145, pp. 174–198.

Kundu, P.K. and Cohen, I.M., 2008. *Fluid Mechanics*. Elsevier Academic Press, Oxford, 4th edition.

Kundu, P.K., Cohen, I.M. and Dowling, D.R., 2015. *Fluid mechanics*. Academic press.

Lefebvre, A.H. and McDonell, V.G., 2017. *Atomization and sprays*. CRC press.

Marchione, T., Allouis, C., Amoresano, A. and Beretta, F., 2007. "Experimental investigation of a pressure swirl atomizer spray". *Journal of Propulsion and Power*, Vol. 23, No. 5, pp. 1096–1101.

Schmid, P.J. and Henningson, D.S., 2001. *Stability and Transition in Shear Flows*, Vol. 142 of *Applied Mathematical Sciences*. Springer, New York.

8. RESPONSIBILITY NOTICE

The authors are the only responsible for the printed material included in this paper.